Naeimeh Jafarifar, Kypros Pilakoutas, Terry Bennett
Moisture transport and drying shrinkage properties of steel-fibre-reinforced-concrete
Construction and Building Materials, 2014; 73:41-50

Moisture transport and drying shrinkage properties of Steel-Fibre-Reinforced-Concrete

Naeimeh Jafarifar [a], Kypros Pilakoutas [b], Terry Bennett [c]

[a, b] Department of Civil and Structural Engineering, University of Sheffield, Sir Frederick Mappin Building, Mappin Street, Sheffield, S1 3JD, UK

[c] School of Civil, Environmental and Mining Engineering, Engineering North N136, North Terrace Campus, The University of Adelaide, SA 5005, Australia

[a] Corresponding author: Tel.: +44 (0)114 222 5724, n.jafarifar@sheffield.ac.uk

[b] k.pilakoutas@sheffield.ac.uk

[c] terry.bennett@adelaide.edu.au

Abstract

Drying shrinkage has a serious impact on the structural and durability performance of concrete pavements. Shrinkage strain development and distress can only be fully understood by knowing the moisture transport and free shrinkage properties of concrete. This paper uses experiments and FE inverse analysis to determine these properties for conventional concrete (CC) and RCC reinforced with recycled-steel-fibres from tyres. Moisture diffusivity versus moisture content and a relationship between free shrinkage and moisture loss are derived. These values can be used to predict shrinkage strains and stresses in road pavements and other ground restrained slabs.

Keywords: Drying Shrinkage; Moisture Transport; Recycled Fiber; SFRC; RCC; Pavement.

1 Introduction

In studying drying shrinkage, it is important to understand and quantify moisture movement in concrete during drying [1, 2, 3]. When concrete dries, the pore water moves towards the surface through the pore network and this results in variable moisture content in space and time. Moisture transport in concrete is more complex than in other porous media, as it has a wide variety of pore structures and the pore structures themselves change with time [4].

Drying shrinkage is critical for concrete pavements due to their large surface area. In particular, it significantly affects the performance and life time of concrete roads [5]. It has

CC: Conventional concrete
FE: Finite element
RCC: Roller-compacted-concrete
RTSF: Recycled-tyre-steel-fibres
SFRC: Steel-fibre-reinforced-concrete
SFR-CC: Steel-fibre-reinforced conventional-concrete
SFR-RCC: Steel-fibre-reinforced roller-compacted-concrete

been demonstrated numerically by the authors [6] that shrinkage induced internal strains and cracking can reduce the effective design stress used in pavements by up to 50%. For jointless SFRC pavements, shrinkage is the main limiting factor that determines the size of the slab. The same applies to RCC which can be used as an alternative to asphalt roads, or SFR-RCC in which the roller-compaction construction technique is used for placing SFRC. Early shrinkage behaviour of RCC is reported to be quite different to that of CC [7]. The few published investigations report that drying shrinkage of RCC is relatively low compared to CC [8, 9]. This is attributed to its lower moisture content or lower paste content. Whilst less paste in RCC can help to reduce the volumetric changes induced by drying, more voids and pores due to the nature of RCC may also change the moisture transport and shrinkage properties. Fibres can also change the pore structure of the concrete and affect the moisture transport and drying shrinkage [10]. Published research work on RCC and SFR-RCC does not deal with moisture transport and shrinkage properties.

Using fibres in concrete leads to increased strain capacity and energy absorption by controlling crack propagation. Many different types of fibres have been used in concrete, but steel fibre is the most common. Steel fibres are produced in different shapes and lengths. The ability of fibres to bond with the concrete depends on the aspect ratio of the fibres and the surface characteristics. Thinner steel fibres could bridge microcracks more effectively and influence positively the early-age shrinkage of concrete. Such fibres can be obtained from recycling post-consumer tyres and can contribute to making SFRC more economical and environmentally friendly [11]. Recycled-tyre-steel-fibres (RTSF) have been developed at the University of Sheffield and examined extensively during the EU collaborative research project, Ecolanes [6, 12, 13, 14, 15, 16]. The work reported in this paper was part of Ecolanes and contributed to the development of numerical models for the analysis of road pavements. The objective of this work was to determine the moisture transport and shrinkage properties of CC and RCC reinforced with a practical content of steel fibres recycled from post-consumer tyres (2.5 % by weight) for FE modelling and comparison and design purposes. The material properties which are directly involved in the drying procedure of concrete are moisture diffusivity, convective moisture transport coefficient (also called film factor or surface factor) and hygral contraction coefficient (also called shrinkage coefficient) [17, 18]. These properties cannot be determined from the simple ring tests and in this paper special experimental procedures are adopted and modified to determine them. The approach followed in this paper is based on a combination of experimental studies and inverse analysis techniques. During the inverse analysis (or back-calculation), the properties are changed in a FE model so as to achieve iteratively the same moisture profiles or shrinkage history as obtained from experiments.

The paper begins by reviewing the factors involved in moisture transport and drying shrinkage of concrete. The moisture measurement methods are then evaluated to plan the experimental programme. The experimental procedures are presented followed by numerical inverse analysis and results.

2 Factors involved in moisture transport and drying shrinkage of concrete

In porous media, moisture can flow partly as liquid in capillaries and partly as vapour. In soil, the water movement happens distinguishably with both mechanisms (bulk water and vapour flux). Bulk water flux is controlled by pore water suction and elevation potential (capillary action). Vapor flux is governed by vapor diffusion in unsaturated pore space [1].

In concrete, when pore relative humidity is in the range of 15 to 95%, moisture movement in the form of vapour flux is dominant [19]. Therefore, the flow of moisture in concrete subjected to drying is in general assumed to obey the diffusion principles [1, 2, 3, 17, 19, 20, 21, 22, 23, 24], especially when the moisture content decreases below 70 to 80% of initial saturation [25].

The first application of diffusion principles in a study of moisture distribution in concrete was reported in 1937 by Carlson [20]. Pickett [21] in 1946 revealed that the diffusion equation describing moisture movement in concrete can be equivalent to the equation of heat conduction. However, the order of magnitude of the corresponding coefficients for diffusion of heat and diffusion of moisture are entirely different. Using this approach, only one material property, diffusivity, is involved in characterising the moisture movement within concrete, which makes it very convenient for analysis.

2.1 Diffusion coefficient

Assuming that the diffusion theory applies, the transport of moisture in concrete is governed by Fick's second law [17, 23], details of which are given in Appendix A.

To determine the moisture diffusivity, K_C, as a material property, moisture measurements should be taken from drying specimens as a function of time and depth. Based on experimental moisture profiles, the diffusivity equation can be solved numerically or analytically to obtain the relevant moisture diffusivity. Different forms of analytically or empirically estimated closed-form functions defining the dependency of K_C on the moisture content, C, have been introduced in the literature [2, 3, 5, 10, 18, 22, 26].

In an approach proposed by Sakata [2] and adopted by others [1, 23, 24, 26], by assuming one-dimensional moisture transport the diffusion equation can be solved (Eq. 1) using Boltzman's transformation, $\tau(x , t) = x /\sqrt{t}$.

$$K_C]_{C=C1} = (-1/2 \int_1^{C1} \tau . \mathrm{d}C) / (\mathrm{d}C/\mathrm{d}t]_{C=C1}) \qquad \text{Eq. 1}$$

Initial condition: $C = 1$ for $x > 0 , t = 0$

Boundary condition: $C = C_1$ for $x = 0 , t > 0$

Where, x is the distance from the drying surface and t is the drying time.

Since the slope of the curve $C(\tau)$ is very sharp at the beginning of drying, small inaccuracies in estimating the function $C(\tau)$ from experimental data can make a big difference on the resulting derivative to be used in Eq. 1. This affects significantly the calculated K_C at the beginning of drying. Therefore, this method is not generally satisfactory and some scholars have suggested adopting numerical inverse analysis instead [3, 4] to obtain K_C.

Vapour transfer in air occurs with a diffusion coefficient of about 218 mm^2/day at 20 ºC, that is nearly 50 to 100 times faster than in concrete [18]. This upper limit has not been respected in values determined by some researchers (e.g. [1, 23]), proposing values up to 10000 mm^2/day for the diffusion coefficient in concrete. Based on the values proposed by other researchers [2, 18, 22, 27], the diffusion coefficient in concrete reaches maximum values between 20 to 100 mm^2/day at 100% moisture content. In some studies a constant value has been determined for the diffusion coefficient of concrete (the constant value of 9.29 mm^2/day by Carlson [20] and the value of 23 mm^2/day by Pickett [21]), while an S-shape curve has been proposed in other references [2, 19] to express the variation of the moisture diffusivity with the moisture content. These differences in values proposed in the literature are large enough to change completely the drying pattern in concrete. Hence, for the particular concrete mixes studied herein the diffusion coefficient will be determined from experimental measurements combined with inverse FE analysis.

2.2 Convective moisture transfer coefficient

Convective moisture transfer coefficient, f, deals with the moisture exchange between the concrete surface and the atmosphere. It depends on the water-cement ratio, w/c [2], the moisture gradient, the surface texture and the speed of air flow. However, the overall effect of the environment on f is negligible [18]. For normal concrete, f was found by Sakata [2] to be in the range of 0.75 mm/day to 7.0 mm/day; a very wide range of values. To improve the

accuracy of predictions, for the particular concrete mixes studied in this paper, f will be calculated by inverse FE analysis.

2.3 The relationship between free shrinkage strain and moisture loss (Hygral contraction coefficient)

This relationship is a material property applicable for any shape of concrete member with any type of restraint. Free shrinkage strain is normally given as a nonlinear function of drying time and ultimate shrinkage (e.g. in [28, 29]). Ultimate shrinkage strain is usually a function of ambient relative humidity, initial curing condition, volume to surface ratio, concrete composition, air content and percentage of fine aggregates. These factors indirectly alter ultimate shrinkage strain by affecting the moisture movement in the concrete and the resultant moisture content at any given time, t. Therefore, it is simpler to directly relate free shrinkage strain to relative moisture content. The relationship between moisture loss and free shrinkage strain is nonlinear [17], although it was initially thought by researchers to be linear (e.g. [21]). Ayano et al. [18] proposed a power function for this relationship.

To quantify shrinkage as a material property, concrete should be stress-free or unrestrained. Concrete dries slowly from the surfaces, which means it dries non-uniformly during the experimental time period. This invariably leads to a moisture gradient and consequently a shrinkage gradient develops through the section of the specimen.

Direct measurement of free shrinkage in sizeable concrete elements is not straightforward for two reasons: 1) Due to non-uniform drying, measured shrinkage varies depending on the location of the measurement; 2) Internal restraint develops due to non-uniform shrinkage leading to tensile stresses on the surfaces and compressive stresses in the core of the specimen. Tensile stresses can restrain free shrinkage on the surface and compressive stresses increase the apparent shrinkage strain of the core. The degree of developed internal restraint depends on the specimen size and aggregate type. Hence, unrestrained drying shrinkage can only be measured on small specimens with a thickness of a few millimetres [30]. Small specimen sizes are suitable for cement-paste materials, but not for concrete with normal aggregates and particularly for RCC.

In this study inverse analysis is adopted to calculate the relationship between free shrinkage strain and moisture content from experimental measurements on sizeable prismatic specimens. In this case, FE analysis deals directly with the issue of internal restraint due to the moisture gradient. Hence, it is possible to obtain free shrinkage properties even from the experimental results on sizeable specimens. Since the duration of experimental

measurements is relatively short, intrinsic creep or the viscous behaviour of concrete under sustained stresses is ignored.

3 Experimental study

3.1 Mix proportions and characteristics

Two plain mixes and two SFRC mixes were cast including both RCC and CC mixes. Mix proportions, typical of UK practice, are shown in Table 1. A sulfo-aluminate low energy cement was adopted to reduce environmental impact. The air content of the CC mixes was 5% and the target slump was 70 mm.

Table 1 Proportions used for concrete mixes

Mix	Cement (kg/m^3)	W/C	Crushed aggreg. (kg/m^3)	River aggreg. (kg/m^3)	Sand (kg/m^3)	Superplasticizer[a]	Air-entrainer[a]
CC	380	0.35	-	1004	833	0.85%	0.135%
RCC	300	0.54	2084	-	-	-	-

[a] % by cement mass

The fibre content used for SFRC mixes was the optimum practical amount for recycled fibres determined by the Ecolanes [12] project (60 kg per each cubic meter of concrete or around 2.5% by weight). The statistical length distribution of RTSF used is this study is shown in Fig. 1 (85% of the fibres had length in the range of 10 to 25 mm, and 50% of them in the optimum range of 15-25 mm). These comply with Class A RTSF as defined by Ecolanes [12]. These fibres had diameter in the range of 0.1 to 0.23 mm and a tensile strength of around 2000 MPa.

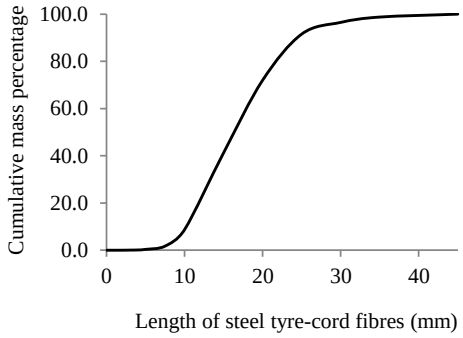

Fig. 1 Statistical length distribution of steel tyre-cord fibres used in SFRC mixes

The aggregates used for CC mixes were river aggregates. Graded crushed granite was used for the RCC mixes, as is the normal practice in the UK, to increase the bond between the paste and aggregate and to provide stability during rolling. To avoid balling and to optimise the use of fibres in concrete, it is normally recommended that the nominal maximum size of coarse aggregate is less than 2/3 of the dominant fibre length [31]. As a result the nominal maximum size of aggregates was limited to 14 mm. The aggregate gradation is shown in Table 2. This gradation complies with the bounds adopted by industry in the UK. The

aggregates were stored indoor prior to mixing in a dry condition with an environmental humidity of about 40%.

Table 2 Gradation of aggregates used for CC and RCC mixes

gradation (mm)	CC mixes		RCC mixes
	Sand (%)	Coarse agg. (%)	Crushed agg. (%)
9.5-14	-	10	21.5
4.75-9.5	2	80	21
1.18-4.75	26	10	19.5
0.5-1.18	32	-	10.5
0.15-0.5	37	-	14
.075-0.15	2	-	7
< 0.075	1	-	6.5

For CC the recommendations of the BS 8500-1 [32] were used to develop a designated PAV2 mix which is an accredited mix that can be used for heavy-duty external paving for rubber tyre vehicles. Since steel fibres are randomly distributed inside the concrete, the mix was designed to comply with the minimum cover requirement. Considering cyclic wet and dry conditions for pavement applications with an intended working life of at least 50 years, a cement content of 380 kg/m3 and a water-cement ratio of 0.35 were required to fulfill the minimum cover requirements.

For the RCC mix design, the cement content of 300 kg was selected to achieve the same strength as for CC. The RCC water content was optimized to yield the maximum dry density for the compacted mix (7% by mass for the used cement and aggregates).

RCC has generally lower cement content and reduced amount of water compared to CC. However, for SFR-RCC enough paste should be provided to enable adequate fibre bond. For CC, super plasticizer was used to reduce water demand; this was not possible for RCC.

A specially designed device having a fixed weight and a 1.6 kW electric vibrating hammer (16 to 32.5 Hz) was used for compaction of RCC specimens. RCC specimens were cast in three layers each compacted for 60 seconds. The 28 day compressive strength, obtained from 150 mm cubes, is given in Table 3.

Table 3 Average 28-days compressive strength

	Compressive strength, MPa	
	CC mixes (SD)	RCC mixes (SD)
Plain concrete	58 (1.6)	49 (1.7)
SFRC	61 (0.0)	51 (1.0)

3.2 Moisture measurement in concrete

For one dimensional moisture transport, two methods are usually used to measure the depth distribution of moisture as a function of time: 1) A method using small probe-type sensors

embedded in the concrete specimens at different distances from a surface exposed to drying; 2) The gravimetric method.

Embedded sensors usually need longer time to stabilise their reading, hence they are not suitable in the early stages when moisture content drops sharply. In the conventional gravimetric method [2, 3, 23, 24, 25], specimens of different heights are cast (Fig. 2) and their weight changes are measured in frequent time steps to determine loss of moisture through the depth. As a result, this method does not account for moisture exchange from the underlying depth of concrete as it assumes that the moisture content at any given depth is independent of the total height of the specimen. In this study, the conventional gravimetric method has been modified to preserve the original moisture boundary condition from the bottom boundary. In this modified method, all specimens are cast with the same total height and each is sliced at a given depth (h_1, h_2, h_3, etc.), the integrity of specimen is maintained by keeping both segments in contact for the duration of the measurements (Fig. 3).

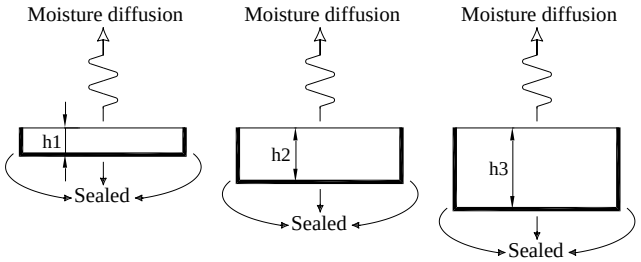

Fig. 2 Specimens in the conventional gravimetric method for moisture measurement

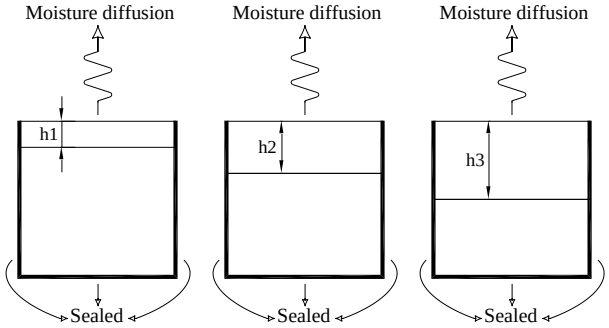

Fig. 3 Specimens in the modified gravimetric method for moisture measurement

Specimens were initially cast in 550×150×150 mm steel moulds and cured in water for 90 days. Each prism was then cut to make three 180×150×150 mm long prisms each sliced in two segments at different depths as illustrated in Fig. 4. Cutting was performed in wet conditions and the specimens were protected from drying before being sealed. The sides of the top and bottom segments were sealed separately (Fig. 5(a), surfaces 1 to 4 in the top segment and surfaces 1 to 5 in the bottom segment), using a high-performance 5 ply laminated aluminum foil tape. This approach was designed to provide one-dimensional

drying conditions. Three specimens were cast for each depth, h_i. After each weight measurement, the two segments were put back together (Fig. 5(b)) and the joint was sealed using a new 75 mm wide plastic tape (Fig. 5(c)). This piece of tape could be easily unwound for the next measurement and was discarded after each use.

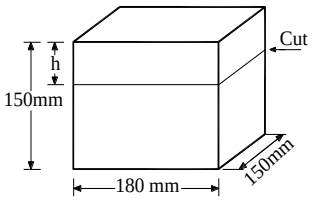

Specimen No.	Cutting depth (h)
1	10 mm
2	20 mm
3	35 mm
4	60 mm
5	100 mm

Fig. 4 Cutting depths in moisture measurement

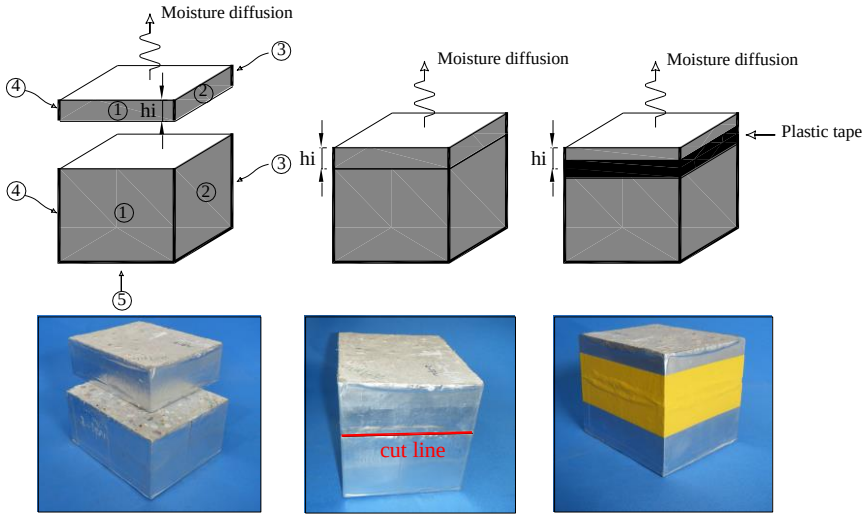

(a) (b) (c)

Fig. 5 Sealing specimens in the modified gravimetric method

The only issue that needs consideration in this method is the effect of the contact between the two segments on moisture transfer. The cut plane may disturb the assumed one dimensional moisture movement. If the gap is considerable, the air layer between discontinuity surfaces may change the rate of moisture transfer. This effect has been studied by Ayano et al. [18], who carried out experiments on specimens prepared by piling up 11 slices 150 × 100 × 3 mm and sealing the outer surfaces, for determination of moisture distribution. For comparison, solid specimens of 150 × 100 × 33 mm were also used with the same sealing conditions. Two solid specimens and nine sliced specimens were put in an environmental chamber with relative humidity of 45% at 20 °C. Drying began at the age of 14 days. Moisture loss was measured at 0.5, 3, 7, 13, 27, 42, 56, 70, and 98 days after the start of drying. At each measurement one of the sliced specimens was used; the sealing foil was removed to obtain the moisture loss of each slice and then the specimen was discarded. The moisture distribution obtained from the piles of sliced specimens was used as a substitute for that of the solid specimens in order to obtain the diffusion coefficient. From

that study, it was found that the effect of cutting the specimens on the moisture flow can be considered to be small.

The specimens were placed in a chamber with relative humidity of 40±3% and temperature of 25±3ºC. Weight changes were measured at frequent time intervals to determine the moisture content over time.

After 84 days of measurements, the specimens were unsealed and put in the oven for a period of seven days at 120ºC. This duration was not long enough to dry the core of the thick specimens, but for the specimens thinner than 35 mm the drying rate approached zero towards the end of the week. Therefore, the dry density of each mix was determined by averaging the dry weight of segments having thicknesses less than 35 mm.

Shrinkage in concrete is due to loss of water either to internal chemical reactions in immature concrete (autogenous water loss) or to the environment (drying). Autogenous shrinkage takes place early and is strongly dependent on the curing conditions; it can be limited by keeping the surface of the concrete continuously wet. On the other hand, drying shrinkage is a long term issue and it is inevitable under normal service conditions. To simplify the interpretation of results, it is easier to assume wet curing and thus do not take into account autogenous shrinkage. To ensure that only drying shrinkage was monitored in the experiments, and there was no significant effect from autogenous and plastic shrinkage, measurements started only after the concrete specimens matured in water for 90 days.

3.2.1 Calculation of moisture content in the gravimetric method

The moisture content, $C(x , t)$, as a percentage of initial diffusible moisture, at any depth x_i (as shown in Fig. 6 (a) and (b)) and at time t can be calculated from Eq. 2 and Eq. 3 [23].

$$C(x_i , t) = [1 - (M_{ti} - M_{t(i-1)}) / (\gamma_{0i} . S. (h_i - h_{i-1})] \times 100 \qquad \text{Eq. 2}$$

$$\gamma_{0i} = (W_{0i} - W_{fi}) / (h_i . S) \qquad \text{Eq. 3}$$

Where h_i is the height of specimen i (top segments) (mm); M_{ti} is the moisture loss in specimen i at time t (kg); S is the area of the drying surface (mm^2); γ_{0i} is the diffusible moisture per unit volume (kg/mm^3); W_{0i} is the initial weight of specimen i before drying (kg); W_{fi} is the dry weight after full drying in the oven (kg).

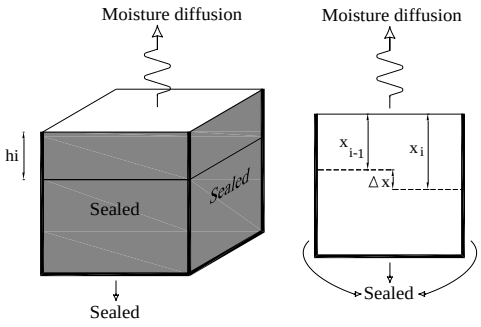

Fig. 6 (a) Specimen *i* in formulation of the moisture content; (b) Continuous specimen in formulation of the moisture content

3.3 Free shrinkage measurements

To measure free shrinkage, long prismatic specimens are needed [33, 34]. ASTM C 157 uses specimen size 76 × 76 × 286 mm whilst BS EN 12617-4 uses 40 × 40 × 160 mm. In this study, to eliminate the effect of boundary conditions on fibre distribution and due to limitations in compacting RCC in small moulds, the size of specimens was increased to 150 ×150 × 550 mm. The two end sides of the specimen were sealed thus moisture transport was only allowed from the exposed sides (Fig. 7). To provide uniform drying and unrestrained conditions, the specimens were rested on two sharp edges whilst drying (Fig. 8). The length changes were measured over time, using a specially developed Vernier type device with an accuracy of ±0.02 mm. The environmental conditions were the same as those for the specimens in moisture measurement (see Section 3.2).

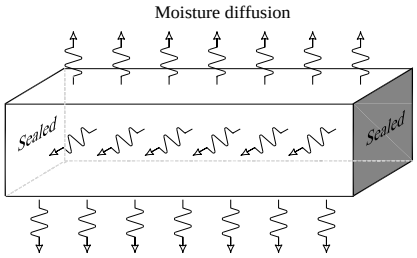

Fig. 7 Prismatic specimen for free shrinkage measurement

Fig. 8 Free shrinkage specimens

3.4 Experimental results and discussion

Fig. 9 shows the time histories of moisture profiles derived from moisture measurements for each concrete mix. Each curve represents the mean value taken from three samples (COVs up to 0.15 but mostly up to 0.04). These results show that the penetration of the drying front in concrete is so slow, such that after around 84 days drying at 40% environmental humidity, the moisture content at a depth of 10 mm from the drying surface only dropped in the range of 65-70%, whereas, at a depth of 35 mm the moisture content remained above 90%. The fastest rate of drying occurs at early ages and then it decreases with time. RCC and SFRC mixes dry faster than CC and plain mixes, respectively, due to their higher porosities. The experimental moisture profiles are used in Section 4.3.1 and 4.3.2 to back-calculate moisture diffusivities, $K_C(C)$, and surface factors, f, respectively.

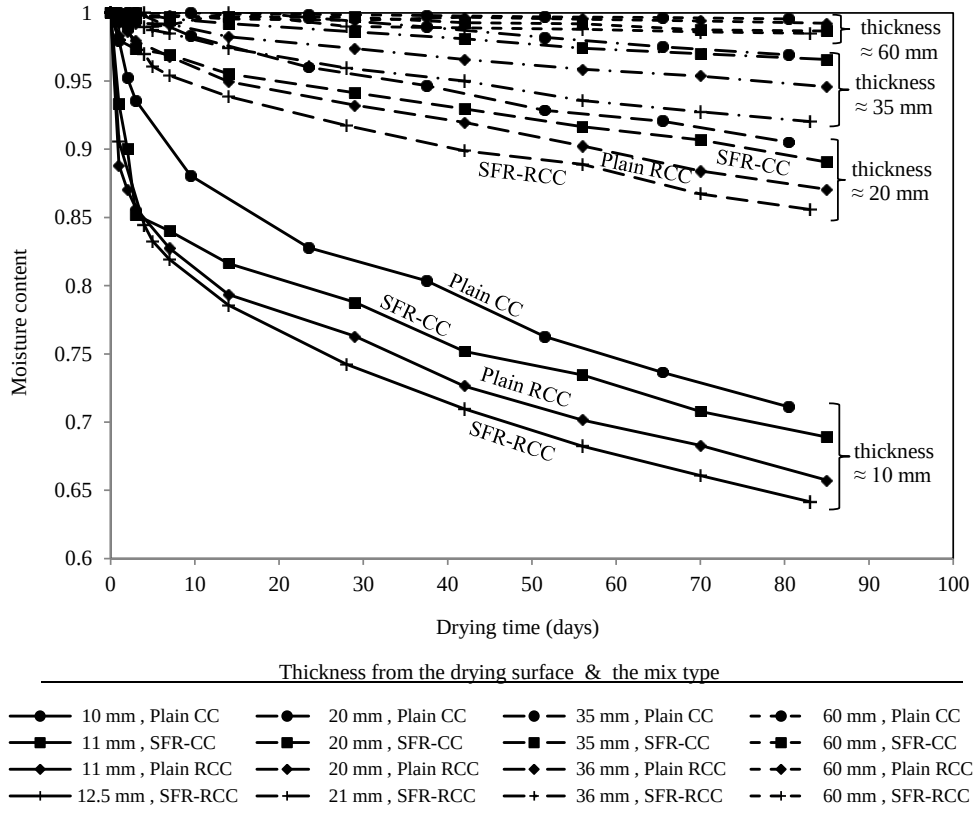

Fig. 9 Experimental moisture profiles

Free shrinkage test results in terms of shrinkage strain versus drying time are presented in Fig. 10. For RCC mixes, shrinkage occurs at a relatively uniform rate. For CC mixes, shrinkage occurs at a fast rate at early ages and then the rate considerably decreases. This results in a lower short-term shrinkage for RCC compared with CC, as reported in the literature. However, the results show that at the end of the measurement period shrinkage of the RCC mixes exceeds that of CC mixes. Free shrinkage test results are used in Section 4.3.3 to back-calculated the hygral contraction coefficients, $\beta_C(C)$.

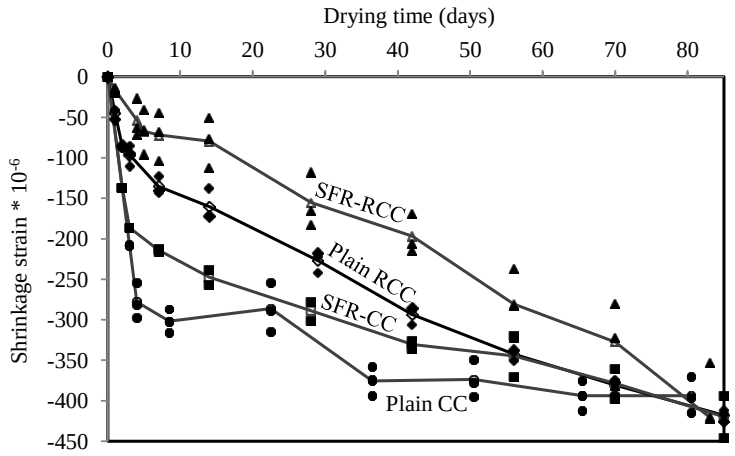

Fig. 10 Strain history curves for free shrinkage specimens

4 Numerical study

4.1 Analysis approach

For numerical analysis, the authors used the FE package ABAQUS [35]. Although ABAQUS has the ability to model deformable porous media [35, 36], the number of parameters that need to be determined can be prohibitive. As mentioned in Section 2, moisture movement in the form of vapour flux is dominant, thus the drying mechanism may be simplified (assuming Fick's second law), requiring only two parameters. Whilst the moisture diffusion option is not available in ABAQUS, the heat transfer option is. Therefore, the heat transport module of ABAQUS was exploited due to the analogy between the governing diffusion equations, with a simple substitution of parameters. This was coupled with structural analysis to calculate shrinkage deformations. Free moisture content was replaced by temperature, moisture diffusivity by thermal conductivity, and hygral contraction coefficient by thermal coefficient of expansion. To avoid the effect of extra multipliers which are needed in the heat transfer equation, but not in the moisture transport equation, specific heat and density were taken equal to unity. By using inverse analysis for each concrete mix, moisture diffusivity and surface factor were back-calculated from the moisture measurement test results, and hygral contraction coefficient from free shrinkage measurements. During the inverse analysis, the mentioned properties were optimised manually to minimise the difference between the experimentally measured moisture profiles and shrinkage histories and those from the model. 3-D, 8-noded solid elements were used for modeling as shown in Fig. 11; DC3D8 for thermal analysis and C3D8 for structural analysis. In modeling free shrinkage, only half prisms were modelled due to symmetry, as seen in Fig. 11(b).

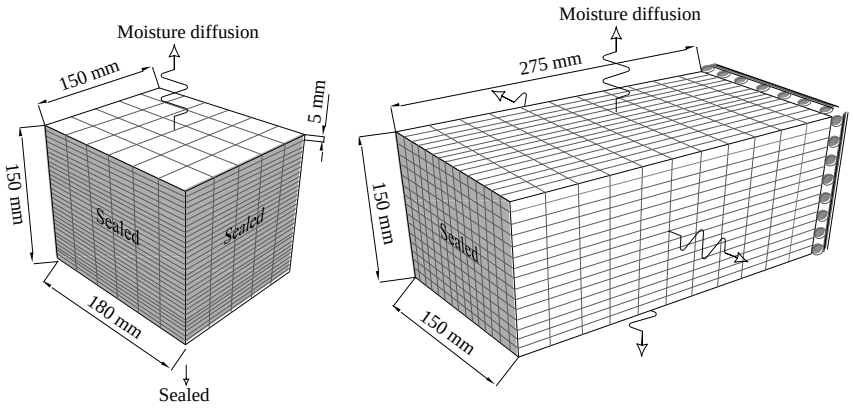

Fig. 11 FE model (a) Moisture measurement specimens, (b) Free shrinkage prisms

4.2 Boundary and initial conditions

A constant ambient humidity of 40% was considered, and moisture convection from the exposed surfaces was taken into account by a surface factor, as described in Section 2. The sealed surfaces were assumed not to have any moisture interaction with the surrounding environment. At time zero, the specimens were fully saturated.

4.3 Numerical results and discussion

4.3.1 Determination of moisture diffusivities

The back-calculated moisture diffusivities, $K_C(C)$, as functions of moisture content, C, derived from experimental moisture profiles, are shown in Fig. 12 for different mixes. Moisture diffusivities vary in the range of 0-5 mm^2/day for moisture content lower than 87-92% and then increase sharply. The moisture diffusivity of RCC mixes is slightly higher than that of CC mixes, and of SFRC mixes slightly higher than of plain mixes. This may be due to the higher porous nature of RCC and air trapped around fibres for SFRC.

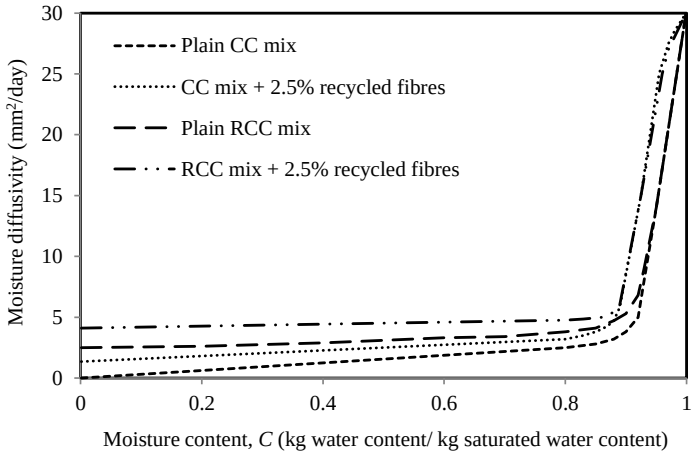

Fig. 12 Moisture diffusivity, $K_C(C)$, versus moisture content, C

4.3.2 Determination of surface factors

The surface factors, *f*, derived from experimental moisture profiles by inverse analysis, were found to be in the range of 3-10 mm/day for CC mixes, and 5-10 mm/day for RCC mixes. Surface factors can significantly affect the moisture profiles near the drying surface. Away from the drying surface, the effect of surface factor on the moisture profiles diminishes quickly, as shown in Fig. 13. To improve the accuracy of the back-calculated surface factors, the experimental values of moisture variation at very close distance from the drying surfaces are required, which are not always possible to measure. However, the accuracy of surface factors in the calculated ranges does not appear to have any significant effect on the moisture profiles, especially at the end of the drying period.

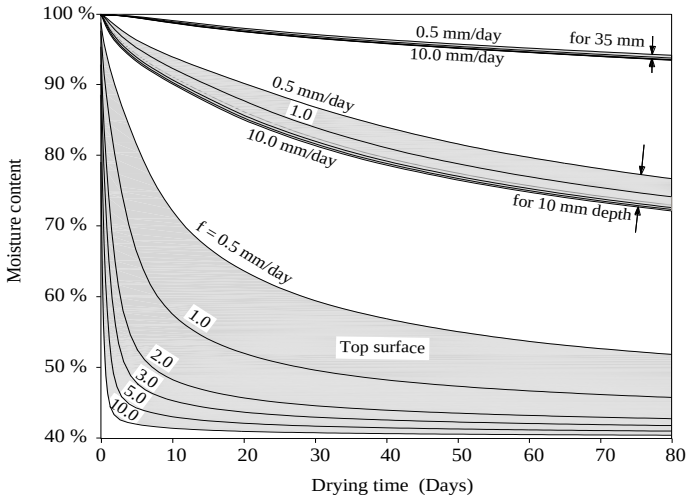

Fig. 13 The effect of various surface factors, *f*, on the moisture profiles at different depths for RCC specimens

4.3.3 Determination of the hygral contraction coefficient

The hygral contraction coefficients, $\beta_C(C)$, were back-calculated as functions of moisture content, *C*, using free shrinkage test results. The coefficient $\beta_C(C)$ induces free shrinkage strain, $(\varepsilon_{sh})_C$, in the specimen based on Eq. 4.

$$(\varepsilon_{sh})_C = - \beta_C(C) \times (C_0 - C) \qquad \text{Eq. 4}$$

Where, C_0 is the reference moisture content, 1.0.

A power function was assumed for the variation of $\beta_C(C)$ versus *C* [18], as given in Eq. 5, and the constant parameters, *a* and *b*, were obtained by inverse analysis for the experimental concrete mixes (Table 4).

$$\beta_C(C) = - a \times (C_0 - C)^{b-1} \qquad \text{Eq. 5}$$

Table 4 Back-calculated constant parameters, *a* and *b*

	a	*b*
Plain CC	1100E-6	0.35
SFR-CC	900E-6	0.4
Plain RCC	2500E-6	0.8
SFR-RCC	1900E-6	0.9

The calculated values of $\beta_C(C)$ are shown in Fig. 14, for various concrete mixes. The hygral contraction coefficient of CC is higher than that of RCC for moisture contents higher than 80%, for both SFRC and plain mixes. This can be attributed to the higher restraining effect of crushed aggregates in RCC mixes, the higher percentage of aggregate used and the different pore structure of RCC. For moisture contents lower than 80%, the hygral contraction coefficient of CC reaches that of RCC. The hygral contraction coefficient of SFRC is generally lower than that of plain mixes (RCC and CC). This effect can be attributed to the restraining effect of the fibres and the different pore structure of SFRC. The hygral contraction coefficient obtained by Ayano et al. [16] for a conventional plain concrete is also shown in Fig. 14 for comparison purposes.

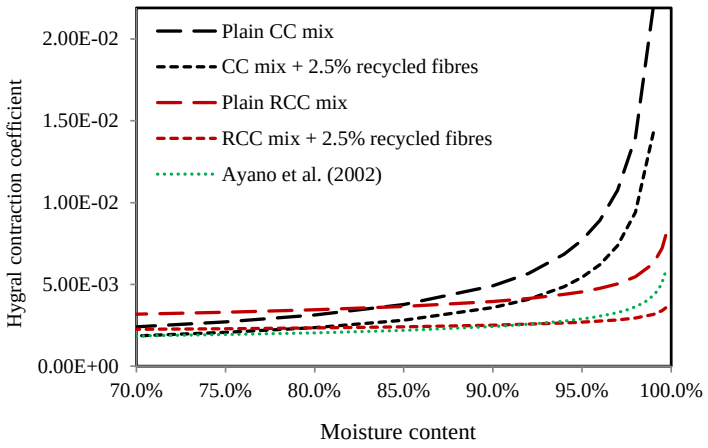

Fig. 14 Hygral contraction coefficients versus moisture content

4.3.4 Comparison with experimental values

4.3.4.1 Moisture profiles

Assuming the moisture diffusivity curves shown in Fig. 12 and the lower limit of the estimated ranges for the surface factors, the numerically calculated moisture profiles are as given in Fig. 15. The curves presented in Fig. 15 are best fit curves to the experimental results (also shown), determined by changing moisture diffusivity and surface factors.

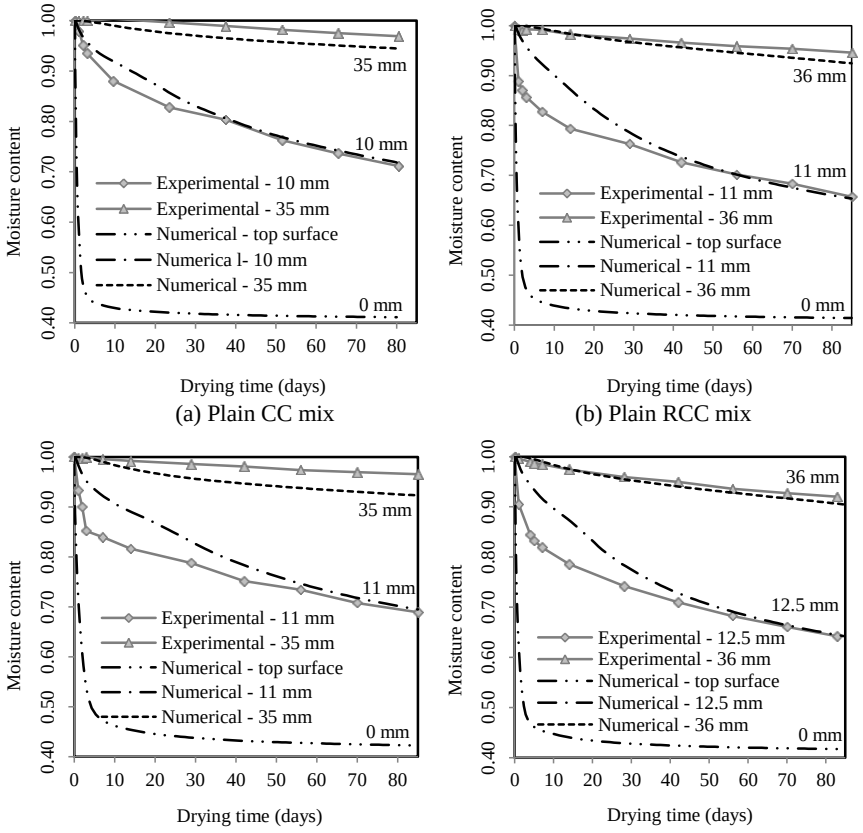

(a) Plain CC mix (b) Plain RCC mix

(c) SFR-CC mix (2.5%) (d) SFR-RCC mix (2.5%)

Fig. 15 Numerical and experimental moisture profiles: (a) Plain CC mix; (b) Plain RCC mix; (c) SFR-CC mix (2.5%); (d) SFR-RCC mix (2.5%)

As seen in Fig. 15, the use of the diffusion theory as the single moisture transfer mechanism in concrete represents satisfactorily the experimental results at moisture contents lower than 75-80%. For moisture contents higher than 80%, the numerically calculated curves do not match the experimental results very well even using alternative profiles for moisture diffusivity. This indicates that for nearly saturated conditions, bulk water flux also participates in moisture transport. This could be the cause of discrepancy at the early drying stage between the experimental curves and numerical curves which have been obtained considering vapour flux as the single moisture transport mechanism. However, even in the worse cases, the difference between the experimental and the numerically predicted values is still limited to 10%.

4.3.4.2 Free shrinkage

Based on the calculated parameters, curves of shrinkage strain versus drying time for free shrinkage specimens are presented in Fig. 16 in comparison with experimental values.

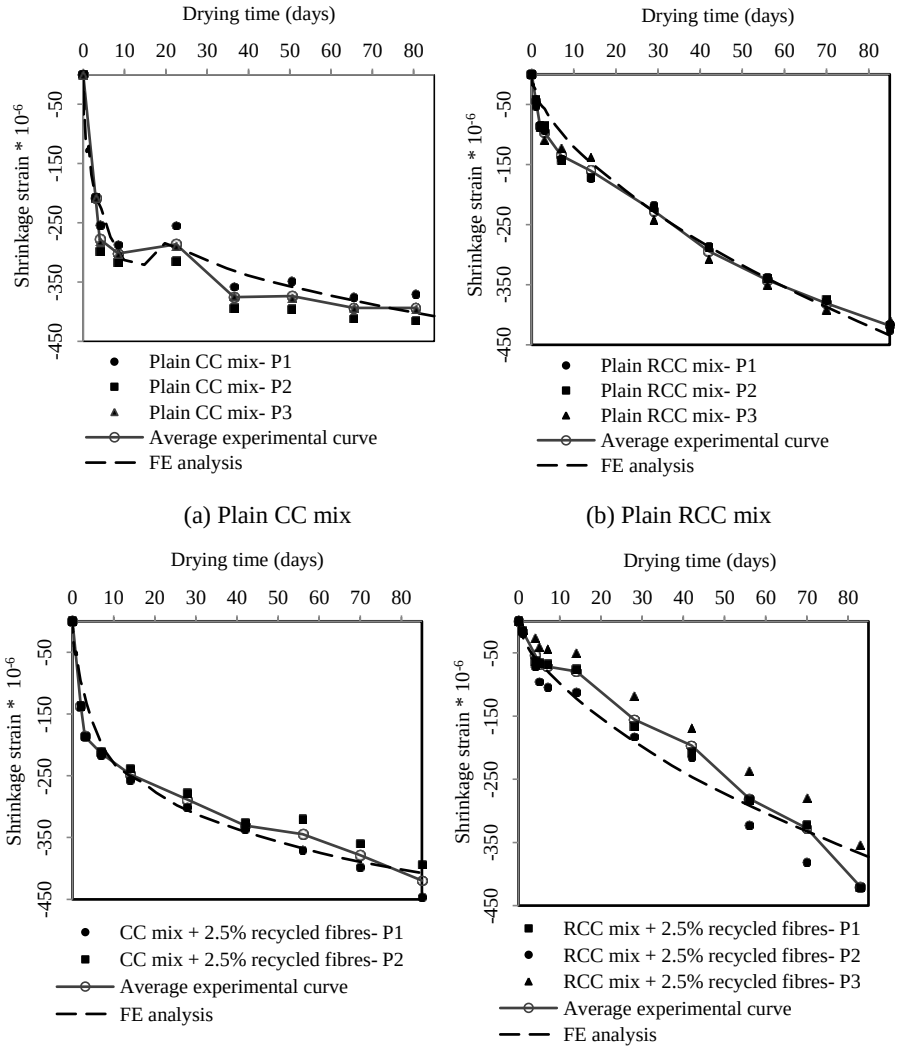

(a) Plain CC mix (b) Plain RCC mix

(c) SFR-CC mix (2.5%) (d) SFR-RCC mix (2.5%)

Fig. 16 Numerical free shrinkage compared with experimental results

In the shrinkage curve of the plain CC mix shown in Fig. 16(a), an unexpected relative expansion is seen around 20 days. This concrete mix is naturally less porous than other mixes, and the results of the hygral contraction coefficient show a sharp decline at high moisture contents for this mix. The relative expansion is observed in 3 tested plain CC specimens as well as in its numerical results. This phenomenon does not seem to be due to an uncontrolled experimental condition, as all the mixes were in the chamber at that time. In the numerical model this relative transient expansion can arise because the hygral contraction coefficient of the plain CC mix rises sharply after 99.9%. As presented in Fig. 17, if the hygral contraction coefficient is limited to the value corresponding to 99.9% moisture content, the expansion does not develop. In sizeable specimen, the sharp decline in the hygral contraction coefficient combined with internal restraints creates tensile stresses moving from the surface inwards with time (as shown in Figure 18). These tensile stresses can lead to a relative small expansion in the specimen between 15 to 20 days, when tensile

stresses arrive close enough to the core. However, further investigations are required to verify experimentally this effect. More experimental tests with different specimen sizes and under various environmental conditions are suggested.

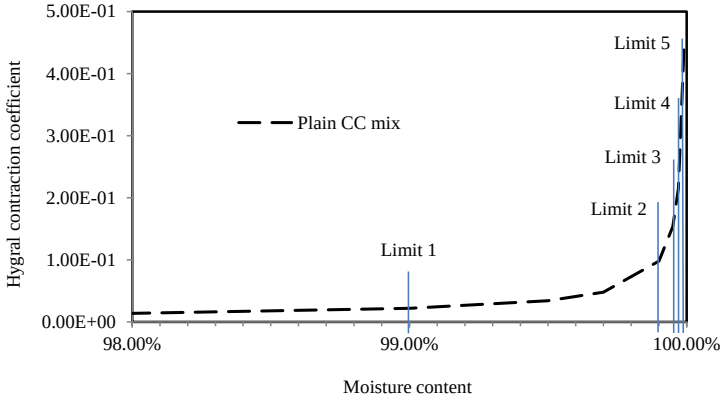

(a)

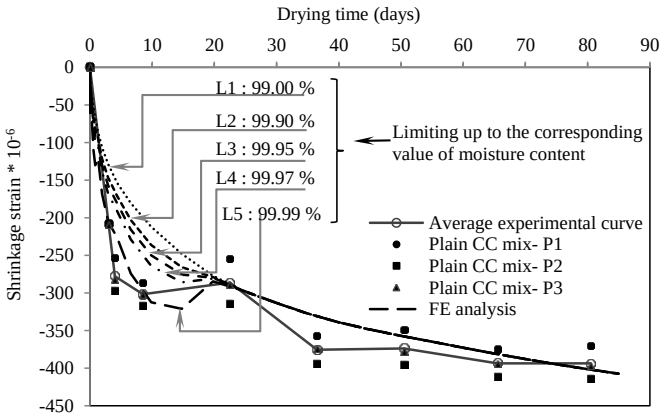

(b)

Fig. 17 Effect of considering upper limit for $\beta c(C)$ for plain CC mix; (a) Limits, (b) Free shrinkage time histories

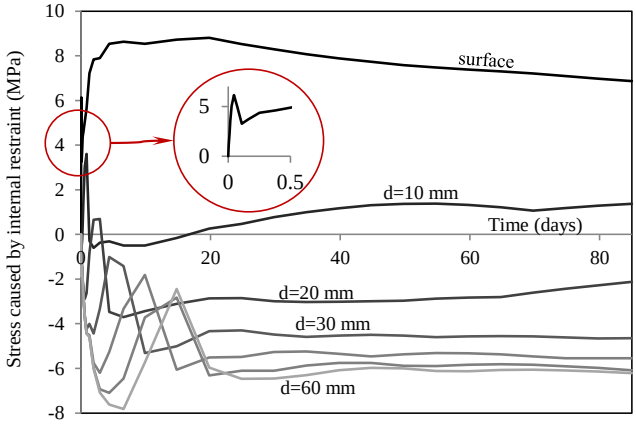

Fig. 18 Tensile wave, moving from the surface inward

5 Conclusions

Moisture transport and drying shrinkage properties were back-calculated for given concrete compositions by inverse FE analysis. The following was found:

- Concrete drying is a very slow process and after 84 days of drying at 40% relative humidity, concrete remained nearly saturated (≈ 95%) at depths bigger than 35 mm from the drying surface.
- The rate of drying is relatively fast at the early ages decreasing with time. Drying in RCC and SFRC mixes is faster than CC and plain mixes, respectively, due to the higher porosity in the former mixes. This results in higher estimated moisture diffusivity for RCC than CC, and slightly higher for SFRC than plain concrete. The moisture diffusivity is in the range of 0-5 mm^2/day for moisture content up to 80% and then rises sharply for all mixes.
- The effect of surface factor on the moisture profiles is only significant near the drying surface; away from the drying surface this effect quickly diminishes.
- At early ages, free shrinkage of CC mixes occurs at a fast rate and then the rate considerably decreases, while for RCC mixes shrinkage occurs at a more uniform rate. This could be a reason for the lower short-term shrinkage reported in the literature for RCC compared with CC. However, in this research at the end of the measurement period, shrinkage of the RCC mixes matched shrinkage obtained for CC mixes.
- The hygral contraction coefficient of SFR-RCC, SFR-CC, plain RCC and plain CC mixes were obtained as a function of moisture content. This coefficient for CC mixes is higher than that of RCC mixes for moisture contents higher than 80%. The reason is the higher restraining effect of crushed aggregates in RCC mixes and the different pore structure of RCC. The hygral contraction coefficient of SFRC mixes is generally lower than that of plain mixes due to the restraining effect of fibres. For moisture contents lower than 80% the hygral contraction coefficients are similar for all mixes in the range of 0.0012-0.0035.

The above material properties are necessary to analyse numerically the performance of concrete pavements and ground restrained slabs. These are used in other work by the authors to assess the combined effect of shrinkage and externally applied traffic load [6].

Acknowledgements

The authors acknowledge the financial support of the 6th Framework Programme of the European Community under contract number 031530.

References

[1] Kodikara J., Chakrabarti S. Modelling of moisture loss in cementitiously stabilised pavement materials. ASCE Int J Geomech, 2005;5(4):295-303.

[2] Sakata K. A study on moisture diffusion in drying and drying shrinkage of concrete. Cem and Concr Res, 1983;13(2):216-224.

[3] Wittmann XH., Sadouki H., Wittmann FH. Numerical evaluation of drying test data. Trans 10th Int Conf on Struct Mech in React Technol, Q 1989:71-79.

[4] Xin D., Zollinger DG., Allen GD. An approach to determine diffusivity in hardening concrete based on measured humidity profiles. Adv Cem Based Mater, 1995;2(4):138-144.

[5] Kwon SH., Shah SP. Prediction of early-age cracking of fibre-reinforced concrete due to restrained shrinkage. ACI Mater J, 2008;105(4):381-389.

[6] Jafarifar N. Shrinkage behaviour of Steel-Fibre-Reinforced-Concrete pavements. PhD thesis. The University of Sheffield, UK, 2012.

[7] Shaw QHW. The early behavior of RCC in large dams. Int J Hydropower & Dams, 2010;17(2):83-90.

[8] Pittman DW., Steven AR. Drying shrinkage of roller-compacted concrete for pavement applications. ACI Mater J, 1998;95(1):19-26.

[9] Delatte N. Simplified design of roller-compacted concrete composite pavement. Transp Res Rec 1896, 2004:57-65.

[10] Li Z., Lara MAP., Bolander JE. Restraining effects of fibres during non-uniform drying of cement composites. Cem and Concr Res, 2006;36(9):1643-1652.

[11] Pilakoutas K., Neocleous K., Angelakopoulos H., Koutselas K. Economical and sustainable pavements - The Ecolanes project. Glob Mag Concr Soc, 2010;44(6):60-61.

[12] Ecolanes (EU FP6 STREP project). Economical and sustainable pavement infrastructure for surface transport. Contract 031530, 2006-2009.

[13] Graeff AG., Pilakoutas K., Neocleous K., Vania M. Fatigue resistance and cracking mechanism of concrete pavements reinforced with recycled steel fibres recovered from post-consumer tyres. Eng Struct, 2012;45:385-395.

[14] Neocleous K., Angelakopoulos H., Pilakoutas K., Guadagnini M. Fibre reinforced roller compacted concrete transport pavements. Transport, 2011;164(TR2):97-109.

[15] Neocleous K., Pilakoutas K. and Tlemat H. Design issues of concrete reinforced with steel fibres recovered from tyres, ASCE Mater J, 2006;18(5):677-685.

[16] Achilleos C., Hadjimitsis D., Neocleous K., Pilakoutas K., Neophytou P., Kallis S. Proportioning of steel fibre reinforced concrete mixes for pavement construction and their impact on environment and cost. Sustainability, 2011;3(7):965-983, ISSN 2071-1050,website.

[17] Rahman MK., Baluch MH., Al-Gadhib AH. Modeling of shrinkage and creep stresses in concrete repair. ACI Mater J, 1999;96(5):542-551.

[18] Ayano T., Wittmann FH. Drying moisture distribution, and shrinkage of cement-based materials. Mater & Struct, 2002;35(247):134-140.

[19] Bazant ZP., Najjar LJ. Nonlinear water diffusion in non-saturated concrete. Mater & Struct, 1972;5(25):3-20.

[20] Carlson RW. Drying shrinkage of large concrete members. ACI J, 1937;33(3):327-336.

[21] Pickett G. Shrinkage stresses in concrete. ACI J, 1946;17(3):165-204.

[22] Bazant ZP., Najjar LJ. Drying of concrete as a nonlinear diffusion problem. Cem and Concr Res, 1971;1(5):461-473.

[23] Asad M., Baluch MH., Al-Gadhib AH. Drying shrinkage stresses in concrete patch repair systems. Mag of Concr Res, 1997;49(181):283-293.

[24] Wong SF., Wee TH., Swaddiwudhipong S., Lee SL. Study of water movement in concrete. Mag of Concr Res, 2001;53(3):205-220.

[25] Selih J., Sousa ACM., Bremner TW. Moisture transport in initially saturated concrete during drying. Transp in Porous Media 24, 1996:81-106.

[26] Penev D., Kawamura M. Moisture diffusion in soil-cement mixtures and compacted lean concrete. Cem and Concr Res, 1991;21(1):137-146.

[27] Yuan Y., Wan ZL. Prediction of cracking within early-age concrete due to thermal drying and creep behavior. Cem and Concr Res. 2002;32(7):1053-1059.

[28] ACI 209R. Prediction of creep, shrinkage, and temperature effects in concrete structures. Amer Concr Inst. Detroit, USA, 1998.

[29] CEB-FIP Model Code (1990). Design code. Comite Euro-Int Du Beton. Thomas Telford, 1991.

[30] Bisschop J. Drying shrinkage micro-cracking in cement-based materials. PhD Thesis, Delft University of Technol., 2002; ISBN 90-407-2341-9.

[31] JSCE-SF1. Recommendation for design and contraction steel fibre reinforced concrete. Jpn Soc of Civ Eng. Concr Libr, 1984;3:5-29.

[32] BS 8500-1. Concrete-Complementary British Standard to BS EN 206-1– Part 1: Method of specifying and guidance for the specifier. Br Stand Inst. London, 2006.

[33] ASTM C 157. Test method for length change of hardened hydraulic cement mortar and concrete. Amer Stand, 2008.

[34] BS EN 12617-4. Products and systems for the protection and repair of concrete structures-test methods - Part 4: Determination of shrinkage and expansion. Br Stand Inst. London, 2000.

[35] ABAQUS Version 6.10. Dassault Systèmes Simulia Corp. USA, 2010.
[36] Lewis RW., Schrefler BA. The finite element method in the static and dynamic deformation and consolidation of porous media. John Wiley, 1998.

Appendix A: Diffusion equation for moisture transport in concrete

The transport of moisture in concrete is governed by Eq. (A.1).

$$\partial C / \partial t = \text{div}\,(K_C(C)\,\text{grad}(C)) \qquad \text{Eq. (A.1)}$$

Where, C is the moisture content which is a function of spatial components and the time from the beginning of the diffusion process, and $K_C(C)$ is the diffusion coefficient. This coefficient is a property of the material and is defined as the rate of moisture flow within the concrete while the moisture gradient is equal to unity. The above equation is strongly nonlinear and the nonlinearity of that is due to high dependency of K_C on the moisture content [19].

For any particular geometry, applying boundary and initial conditions, Eq. (A.1) can be solved for C. For a boundary with surface evaporation Eq. (A.2) applies. With prescribed moisture Eq. (A.3), and for a no flow boundary Eq. (A.4) applies [23].

$$K_C(C)\,\partial C / \partial n = f\,(C_s - C_a) \qquad \text{Eq. (A.2)}$$

$$C = C_b \qquad \text{Eq. (A.3)}$$

$$\partial C / \partial n = 0 \qquad \text{Eq. (A.4)}$$

Where, f is the convective moisture transfer coefficient (also called surface factor or film factor). C_s is the moisture content at the drying surface, C_a is the moisture content in the atmosphere, C_b is the prescribed moisture, and n is the unit normal to the boundary surface.